PHYSICAL REVIEW B **96**, 060410(R) (2017)

SEMPA investigation of the Dzyaloshinskii-Moriya interaction in the single, ideally grown Co/Pt(111) interface

Edna C. Corredor, Susanne Kuhrau, Fabian Kloodt-Twesten, Robert Frömter,* and Hans Peter Oepen
Institut für Nanostruktur- und Festkörperphysik, Universität Hamburg, Jungiusstraße 11, 20355 Hamburg, Germany
(Received 28 April 2017; revised manuscript received 4 August 2017; published 25 August 2017)

The microstructure of magnetic domain walls in epitaxial, single-layer cobalt films on Pt(111) with a pseudomorphic, atomically flat interface is studied by means of scanning electron microscopy with polarization analysis. Uncapped, thermally evaporated cobalt on a clean platinum single-crystal surface is imaged *in situ* in ultrahigh vacuum. For a cobalt thickness of 1.4 nm we observe Néel-like domain walls that show a fixed, counterclockwise sense of rotation. This is indicating a strong Dzyaloshinskii-Moriya interaction (DMI) that originates from the single Co/Pt interface. The width of the domain walls has been determined as $d_w = (27 \pm 2)$ nm. From the observation of a pure Néel-like rotation, we derive a lower bound for the DMI strength of 0.5×10^{-3} J/m^2, which gives a DMI energy per interface atom larger than 0.8 meV. An upper bound for the DMI energy of 4.3 meV per interface atom is derived from the observation of stable domains at the onset of ferromagnetism at 0.3-nm Co thickness, corresponding to an average Co coverage of 1.5 monolayers.

DOI: 10.1103/PhysRevB.96.060410

Introduction. Recently, the Dzyaloshinskii-Moriya interaction (DMI) [1,2] has gained much attention in the field of thin magnetic films with perpendicular anisotropy. In these systems the DMI is caused by spin-orbit coupling (SOC) in the presence of a broken inversion symmetry at the interface between a ferro- and a nonmagnetic layer [3]. Being an antisymmetric exchange interaction, the DMI supports a noncollinear order, leading to new magnetic states, such as magnetic skyrmions, which are promising for the next generation of data storage devices [4].

Even when the DMI is not large enough to stabilize a topologically protected state, it still can have a significant impact on the domain walls of a multidomain state as it causes an additional contribution to the domain-wall energy. Generally, in magnetic films with perpendicular anisotropy uncharged Bloch walls are favored energetically where the magnetization rotates on the wall plane. In the presence of a sufficiently strong interface DMI the magnetization rotates perpendicular to the wall plane, and Néel-like domain walls are observed [5,6]. A fingerprint of such DMI-controlled walls is the fixed rotational sense of all domain walls, which is determined by the sign of the DMI strength D [5]. The fixed sense of rotation ensures a current-induced parallel movement of all domain walls under spin-Hall-effect torque [7]. This makes that wall type interesting for applications in spintronic devices [8].

As a consequence of large DMI, skyrmions that are stable up to room temperature (RT) have been found in several Co-based multilayer systems [9–12]. Maximizing the effective DMI is performed by adding constituents with large SOC and inverse signs of DMI on top and underneath of the magnetic layer. *Ab initio* calculations predict a strong anticlockwise DMI for cobalt on Pt(111) [13–15], which is the common model system for DMI. The effect of the total DMI on domains and domain walls has extensively been studied for polycrystalline multilayers of Pt/Co/Pt, Ir/Co/Pt and Pt/Co/Ir [16–22].

Experimentally, it is not possible to separate the effects of both individual interfaces when trilayers or multilayers are studied. Also, any capping on the system might lead to a change in the total DMI, making an experimental disentangling of DMI contributions necessary. Although not expected in the Fert-Levy model [3], even an oxide-based capping of the cobalt (for instance, in MgO/Co/Pt) results in an additional DMI contribution, which recently was shown experimentally [10] and in first-principles studies [10,23]. In contrast, an uncapped Co/Pt sample is not expected to have an additional DMI contribution from the Co/vacuum interface [23].

Previous studies on the magnetization in epitaxial Co/Pt(111) report the onset of the spin-reorientation transition to an easy plane between 4- and 10-monolayer (ML) Co [24–28]. The monolayer Co/Pt(111) has been studied by spin-polarized scanning tunneling microscopy (SP-STM) [29]. All these studies have been performed however disregarding the effects of DMI. In this Rapid Communication, we show images of the domains and domain walls in epitaxial cobalt films grown on a bulk Pt(111) single crystal at room temperature. The DMI as an interface effect depends strongly on the quality of this interface. Using a single-crystalline substrate we can ensure a well-defined long-range (111) order of the Pt surface. Cobalt was evaporated thermally under ultrahigh vacuum (UHV) conditions onto the single crystal, which results in an atomically smooth interface with negligible disorder or intermixing effects, as the kinetic energies for thermal evaporation are only around 0.2 eV in contrast to magnetron sputtering with about 2 eV [30]. With an increasing number of layers the interface roughness can even be adding up. Furthermore, instead of a capping layer, which introduces a second interface with less ideal properties, a clean vacuum interface is maintained on top of the cobalt. Thus, it is possible to isolate the DMI of the single Co/Pt interface, bringing our system close to the ideal system that has been studied in first-principles calculations. Our results reveal the presence of Néel-like domain walls instead of Bloch domain walls. Furthermore, we find the same sense of rotation for all walls.

Several techniques are capable of investigating the magnetization orientation of narrow domain walls in ultrathin

*rfroemte@physik.uni-hamburg.de

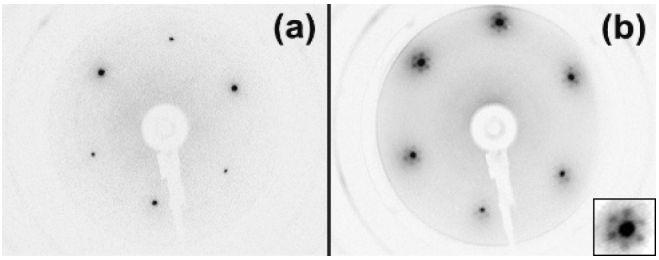

FIG. 1. LEED patterns of (a) the clean Pt(111) surface and (b) a 1.0-nm cobalt film on Pt(111); the fine structure of one of the spots is shown magnified in the inset. The primary electron-beam energy is 80 eV.

films grown on bulk substrates. Spin-polarized low-energy electron microscopy (SPLEEM) [31], x-ray photoelectron emission microscopy [10], and SP-STM [32] can directly image the local magnetization. Via quantitative magnetic force microscopy [9,17,33] and nitrogen-vacancy center microscopy [34,35] a reconstruction of the magnetization from the stray field can be performed. Here we demonstrate the potential of using scanning electron microscopy with polarization analysis (SEMPA). It is a surface-sensitive, vectorial imaging technique with a magnetic probing depth of less than five atomic layers [36] and a spatial resolution down to 3 nm [37]. The capability to measure two components of the in-plane magnetization simultaneously makes SEMPA ideally suited to study DMI effects at the surface of ultrathin magnetic films. In this way, very recently, the absence of DMI in a system was proven by Boehm *et al.* [38]. A statistical analysis of the distribution of local domain-wall angles can be carried out in the same way that has been pioneered using SPLEEM [39]. With the recent development of time-resolved SEMPA, even the recording of magnetization dynamics becomes possible [40].

Experiment. Ultrathin cobalt films were grown on the surface of a bulk (2.5-mm-thick) Pt(111) single crystal by electron-beam (e-beam) evaporation at RT and in UHV (base pressure of 10^{-10} mbar). A clean and atomically flat surface (miscut below 0.1° corresponding to a minimum terrace width of 160 nm) of the single crystal was prepared by repeated cycles of 500-eV (1-μA) argon ion sputtering at RT and subsequent annealing at 900 K for 50 min in an oxygen atmosphere of 2×10^{-8} mbar to remove carbon impurities. Finally, the platinum crystal was flashed to 1050 K to desorb the oxygen layer from the surface. After preparation, a $p(1 \times 1)$ pattern with sharp spots and low background was observed in low-energy electron diffraction (LEED) as can be seen in Fig. 1(a). Cobalt was evaporated by electron-beam heating from a high-purity rod. The deposition rate was 0.07 nm/min, which was monitored during the deposition by maintaining stable conditions of cobalt flux and emission current. For the SEMPA experiments, a wedge-shaped film was grown by using a shutter moving at constant velocity in front of the platinum crystal. This gives continuous access to cobalt thicknesses from 0 to 2.0 nm.

LEED patterns recorded at several cobalt coverages are consistent with previous observations of samples prepared under similar conditions [41]. The first Co layer is known to grow pseudomorphically, i.e., with the bulk lattice constant of Pt, whereas the second layer starts to develop a moiré structure [42,43]. This growth mode is a consequence of the strong lattice mismatch (−9.4%) between Co and Pt as the additional Co layers start to grow with the smaller lattice constant of cobalt. A flat two-dimensional growth of fcc Co nevertheless is reported up to 0.7-nm coverage (3.5 MLs) [42,43]. Between 0.7- and 1-nm Co coverage a sixfold fine structure around the main LEED spots is observed [see Fig. 1(b)], which is indicating the presence of the moiré structure mentioned above. This LEED pattern remains stable up to a thickness of around 1.4 nm (7 MLs). Upon further deposition the pattern becomes blurry due to the growth of triangular-shaped cobalt islands with predominantly fcc-twinned stacking [42]. Regardless of the three-dimensional growth at higher Co coverage, the first monolayer stays two dimensional, preserving the ideally flat interface between Co and Pt.

A primary beam current of 3 nA at 6 keV was used to acquire the domain images via SEMPA. A dwell time of 30 ms yields roughly 15 000 counts per pixel and channel. The image contrast is given by the normalized intensity asymmetry of the (2,0) beams from secondary electrons scattered at a W(001) surface that we use as a spin detector; it is proportional to the local magnetization component [44–46]. Our setup allows for simultaneously measuring two orthogonal in-plane components of the magnetization [47]. The preparation is performed in a vacuum chamber that is attached directly to the SEMPA microscope, thus immediately after Co deposition the sample is transferred under UHV conditions into the microscope chamber (pressure in the low 10^{-11} mbar), and the domain structure is imaged. All experiments are performed at room temperature and in the as-grown state, i.e., without applying external magnetic fields.

Results and discussion. All domain images presented in the following have been taken at a cobalt thickness of 1.4 nm where the easy axis of magnetization points out of the film plane. This thickness has been chosen as at just slightly higher thicknesses (1.5 nm) the spin reorientation transition sets in where the situation gets too complex to be analyzed with the simple models available. At lower thicknesses the domain walls were too small to be analyzed with good accuracy. However, due to the even stronger contribution from the interface we expect the Néel-like walls to persist down to the onset of ferromagnetism. We find the first magnetic contrast at a cobalt thickness of 0.3 nm where domains of roughly 2 μm appear. Figures 2(a) and 2(b) show the measured horizontal and vertical spin-polarization components on the surface plane, respectively. To get access to the perpendicular component of the magnetization, the sample has been tilted slightly with respect to the detector plane so that a contribution of the out-of-plane polarization is added to the vertical channel [48]. Whereas the admixing of the perpendicular component is proportional to the sine of the tilt angle, the in-plane sensitivity shows a cosine behavior, and therefore its reduction can be neglected at small tilt angles.

The images were taken with a sample tilt of 3° around the horizontal axis. From the known tilt direction it is clear that the magnetization of the domains with slightly brighter contrast points out of the substrate (up). Figure 2(c) gives a full three-dimensional map of the magnetization extracted from the

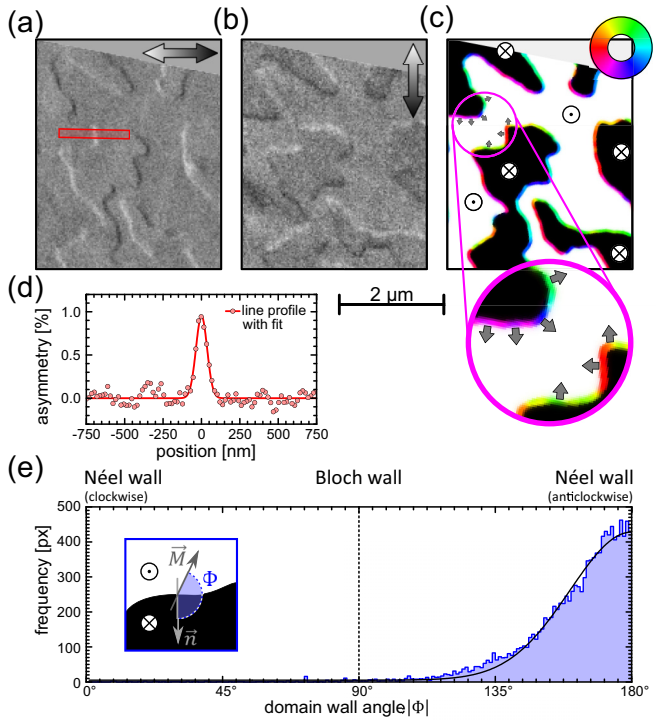

FIG. 2. Magnetic domain structure for a 1.4-nm cobalt layer. (a) Horizontal and (b) vertical in-plane component images of the spin polarization. Due to a sample tilt of 3° a slight out-of-plane contribution is superimposed in (b). From the raw data a complete three-dimensional map of the magnetization vector is assembled in (c). The white and black contrast indicates domains pointing up and down, respectively. The magnetization components on the film plane are color coded with respect to the color wheel in the upper right corner. As highlighted in the magnified circle, only Néel-oriented domain walls with anticlockwise rotational sense are present over the whole image. Frame (d) shows a representative line profile of the Néel-like domain wall at the position marked in red in panel (a). Note that the width of the domain wall is widened by the profile of the primary electron beam. In (e) a histogram of the measured wall angles ϕ (absolute value) with respect to the local wall normal (see the inset) is plotted. The maximum of this distribution is clearly at 180°, indicating Néel-like walls with an anticlockwise rotational sense.

shown raw data. The up (white)/down (black) domain contrast is obtained from the weak contribution of the perpendicular domains observed in (b). The in-plane orientation of the domain-wall magnetization is color coded in (c) according to the color wheel in the upper right corner. It is calculated from the individual component images in (a) and (b). All domain walls point outward of the down domains [black in Fig. 2(c)] and inward of the up domains (white) confirming the Néel character of the walls.

In addition to these qualitative findings, a more quantitative analysis has been performed by studying line profiles across the domain walls. Figure 2(d) shows a representative line profile extracted from the horizontal [Fig. 2(a)] asymmetry image along the marked trace. The line profile has been taken normal to the domain-wall orientation. Note that the finite width of the primary electron beam [49] leads to a considerable widening of the apparent domain-wall profile, so it does not reflect the actual width as will be discussed later on. Following the evaluation from Chen *et al.* [39] the domain-wall angle can be extracted with high accuracy from a wall angle histogram. Figure 2(e) shows such a histogram of the domain-wall angles (absolute values) relative to the local normal vector of the wall as indicated in the inset on the left-hand side. The data have been accumulated from all domain walls in this SEMPA image and fitted with a Gaussian distribution. The fit gives a maximum at 180.0° that is determined with a narrow uncertainty of ±0.9° and corresponds to anticlockwise Néel walls. The relatively wide distribution of detected wall angles of $\sigma = (41 \pm 2)°$ in the image is dominated by the Poisson statistics of the individual asymmetry measurement in relation to the low domain-wall contrast. The observed anticlockwise sequence of domains and walls confirms the positive sign of D in the epitaxially grown Co/Pt(111). This pure Néel character will be used later on to determine a lower boundary of the DMI strength d of the Co/Pt interface.

As mentioned above, the measured wall profile shown in Fig. 2(d) does not reproduce the exact magnetization profile as the lateral resolution of the magnetic images has to be taken into account. The extracted profiles can be described mathematically as a convolution of the real wall profile and the Gaussian profile of the primary beam. For the fit, a Gaussian profile for the wall contrast and an Erf function for the remaining out-of-plane domain contrast (due to the sample tilt) are assumed.

The extracted domain-wall profile reveals a peak asymmetry that is about 0.9%, which is only about 1/4 of the in-plane domain contrast (3.2%) that is obtained for Co films thicker than 2 nm within the same set of experiments. Obviously, the measured wall profiles are smeared out by the finite width of the primary electron beam. As pointed out by Rohart and Thiaville the DMI term does not directly affect the wall width but primarily the in-plane rotational angle [50]. The tiny correction of the domain-wall width predicted by simulation is only a secondary effect of the magnetic charges in the Néel-like wall compared to the uncharged Bloch wall [6,14]. The core regions of the Bloch and Néel-like domain-wall profiles are identical and thus the domain-wall widths are the same. Small differences appear only in the tails of the Néel-like wall, which are, however, not resolved in our measurements. To determine the domain-wall width, we therefore model the profile of the Néel-like wall with a profile of the common Bloch form $Asy = \frac{Asy_{\max}}{\cosh(\frac{x}{\Delta})}$ [51] where $Asy_{\max} = 3.2\%$ is the maximum asymmetry of the spin polarization. The domain-wall width parameter Δ is defined by $\Delta = \sqrt{\frac{A}{K_{\text{eff}}}}$, where A is the exchange stiffness and K_{eff} is the effective anisotropy constant. It can be obtained by fitting the measured domain-wall profile [Fig. 2(d)] with a Gaussian profile,

$$Asy(x) = \frac{V}{\sqrt{2\pi}\sigma} \exp\left[-\frac{1}{2}\left(\frac{x - x_0}{\sigma}\right)^2\right]. \quad (1)$$

The integral over the measured profile $V = (0.86 \pm 0.04)$ nm is set equal to the integral over the ideal domain-wall profile $Asy_{\max}\pi\Delta$, which gives a domain-wall width parameter of $\Delta = (8.6 \pm 0.4)$ nm. This is equivalent to a domain-wall width of $d_w = \pi\Delta = (27 \pm 2)$ nm according to the definition by Lilley [52]. The width parameter results in an effective

anisotropy constant of $K_{\mathrm{eff}} = (0.38 \pm 0.04)$ MJ/m^3 for an exchange stiffness of $A = 28$ pJ/m that has slightly been scaled down from the bulk value to account for the reduced average coordination number of the cobalt atoms [53]. The Co bulk exchange stiffness $A = 30$ pJ/m is taken from literature [54,55]. Moreno *et al.* [56] pointed out a present conflicting situation regarding the use of exchange constants as many publications take only half of the above value (10–16 pJ/m) [11,17,57,58]. Indeed for sputtered systems significantly lower values of A have been reported, depending on the intermixing with other materials [59]. The determination of the DMI strength via static domain size models [11,17] is depending strongly on the used value of A, which causes a systematic deviation in D. The here-obtained value for K_{eff} is reasonable and fits well to reported anisotropies prepared under similar conditions [27].

From the extracted domain-wall information lower (domain-wall angle) and upper (domain-wall width and angle) bounds for the DMI strength D can be determined. As calculated by Tarasenko *et al.* [60], the stray field of a domain wall increases the domain-wall energy σ by

$$\sigma_{\mathrm{stray}} = t_{\mathrm{Co}} \frac{\ln 2}{\pi} \mu_0 M_s^2 \cos^2 \Phi. \tag{2}$$

Here t_{Co}, M_s, and Φ describe the Co thickness (1.4 nm), the saturation magnetization (1440 kA/m [61]), and the in-plane angle of the domain-wall rotation ($0,\pi$ for a pure Néel-like wall with negative, positive D, and $\pm\frac{\pi}{2}$ for a pure Bloch wall), respectively. On the contrary, the DMI energy,

$$\sigma_D = \pi D \cos \Phi \tag{3}$$

results in a reduction of the wall energy, making a Néel-like wall with a fixed sense of rotation energetically favorable. Therefore, for $0 < |D| < \frac{2\sigma_{\mathrm{stray}}(\Phi=0,\pi)}{\pi}$ a smooth transition from Bloch- into Néel-like domain walls takes place on an increase in D [6]. For

$$|D| > \frac{2\sigma_{\mathrm{stray}}(\Phi = 0,\pi)}{\pi}, \tag{4}$$

walls of pure Néel character appear [6], which are found here. Therefore, from the energy balance between DMI and stray field energy $D > 0.5 \times 10^{-3}$ J/m^2 is obtained. As this balance is independent of the exchange stiffness A, the discussed uncertainties in A do not affect the lower bound.

On the other hand, the domain-wall energy density,

$$\sigma = 4\sqrt{A K_{\mathrm{eff}}} + \sigma_{\mathrm{stray}} + \sigma_D \tag{5}$$

has to stay positive as otherwise the system will create spin spirals or a skyrmion lattice as a ground state instead of stable domains [32,50]. The latter condition results in $D < 4.6 \times 10^{-3}$ J/m^2 for 1.4 nm, again using $A = 28$ pJ/m as mentioned earlier. Smaller values of A would lead to a reduction of the upper bound of D. As the DMI originates purely from the interface, both limiting values can be rescaled in terms of DMI energy per interface cobalt atom [13]. In this way, bounds for the DMI strength of 0.8 meV/Co $< d <$ 7.3 meV/Co are derived. As we observe magnetic domains for smaller Co coverage down to 0.3 nm (corresponding to an average Co coverage of 1.5 monolayers) the upper bound can be reduced to 4.3 meV/Co using appropriately scaled values for A and K_{eff} [62]. This range fits to published first-principles calculations for d in Co/Pt systems. Freimuth *et al.* [63] obtain $d =$ 2.7 meV/Co which has been reproduced by Yang *et al.* [64] with $d = 3.1$ meV/Co. Calculations performed by Dupé *et al.* found a DMI strength of $d = 1.8$ meV/Co for the same system [15]. Vida *et al.* [14] obtained a value of $d = 1.98$ meV/Co per bond in the fcc stacking and thus, $d = 6$ meV/Co. The calculated values lie inside the range for stable Néel-oriented walls determined in our experiment. However, using the DMI strength from Vida *et al.* we should observe spin spirals or a skyrmion lattice at 1.5 ML, which is not the case in this experiment.

In conclusion, we have demonstrated the application of SEMPA to the quantitative investigation of interfacial DMI by analyzing the magnetic microstructure at the surface. In the epitaxial, room-temperature-grown UHV/Co/Pt(111) system exclusively Néel-oriented walls appear. The growth and preparation conditions ensure an ideal interface between Co and Pt, making this Rapid Communication comparable to theoretical calculations. The domain walls in the uncapped film of 1.4-nm thickness show a fixed anticlockwise sense of rotation. This result proves that even for thicknesses as high as 1.4 nm the interfacial DMI plays a dominant role despite the $1/t_{\mathrm{Co}}$ decrease in the DMI strength with increasing cobalt thickness. Using the experimentally determined wall angle and width parameter, a span for the DMI strength of 0.8 meV/Co $< d <$ 4.3 meV/Co has been derived, which is largely in agreement with previous *ab initio* calculations for this system.

Acknowledgments. We acknowledge financial support by the DFG within SFB668. We thank Dr. G. Neuber for the additional thickness calibration via ellipsometry.

[1] I. E. Dzialoshinskii, Sov. Phys. JETP **5**, 1259 (1957).
[2] T. Moriya, Phys. Rev. **120**, 91 (1960).
[3] A. Fert and P. M. Levy, Phys. Rev. Lett. **44**, 1538 (1980).
[4] A. Fert, V. Cros, and J. Sampaio, Nat. Nanotechnol. **8**, 152 (2013).
[5] M. Heide, G. Bihlmayer, and S. Blügel, Phys. Rev. B **78**, 140403(R) (2008).
[6] A. Thiaville, S. Rohart, É. Jué, V. Cros, and A. Fert, Europhys. Lett. **100**, 57002 (2012).
[7] S. Emori, U. Bauer, S.-M. Ahn, E. Martinez, and G. S. D. Beach, Nature Mater. **12**, 611 (2013).

[8] S. S. P. Parkin, M. Hayashi, and L. Thomas, Science **320**, 190 (2008).

[9] A. Soumyanarayanan, M. Raju, A. L. G. Oyarce, A. K. C. Tan, M.-Y. Im, A. P. Petrović, P. Ho, K. H. Khoo, M. Tran, C. K. Gan, F. Ernult, and C. Panagopoulos, Nature Mater. (2017), doi: 10.1038/nmat4934.

[10] O. Boulle, J. Vogel, H. Yang, S. Pizzini, D. de Souza Chaves, A. Locatelli, T. O. Menteş, A. Sala, L. D. Buda-Prejbeanu, O. Klein, M. Belmeguenai, Y. Roussigné, A. Stashkevich, S. M. Chérif, L. Aballe, M. Foerster, M. Chshiev, S. Auffret, I. M. Miron, and G. Gaudin, Nat. Nanotechnol. **11**, 449 (2016).

[11] S. Woo, K. Litzius, B. Krüger, M.-Y. Im, L. Caretta, K. Richter, M. Mann, A. Krone, R. M. Reeve, M. Weigand, P. Agrawal, I. Lemesh, M.-A. Mawass, P. Fischer, M. Kläui, and G. S. D. Beach, Nature Mater. **15**, 501 (2016).

[12] W. Jiang, X. Zhang, G. Yu, W. Zhang, X. Wang, M. B. Jungfleisch, J. E. Pearson, X. Cheng, O. Heinonen, K. L. Wang, Y. Zhou, A. Hoffmann, and S. G. E. te Velthuis, Nat. Phys. **13**, 162 (2017).

[13] H. Yang, A. Thiaville, S. Rohart, A. Fert, and M. Chshiev, Phys. Rev. Lett. **115**, 267210 (2015).

[14] G. J. Vida, E. Simon, L. Rózsa, K. Palotás, and L. Szunyogh, Phys. Rev. B **94**, 214422 (2016).

[15] B. Dupé, M. Hoffmann, C. Paillard, and S. Heinze, Nat. Commun. **5**, 4030 (2014).

[16] A. Hrabec, N. A. Porter, A. Wells, M. J. Benitez, G. Burnell, S. McVitie, D. McGrouther, T. A. Moore, and C. H. Marrows, Phys. Rev. B **90**, 020402 (2014).

[17] M. Bacani, M. A. Marioni, J. Schwenk, and H. J. Hug, arXiv:1609.01615.

[18] A. W. J. Wells, P. M. Shepley, C. H. Marrows, and T. A. Moore, Phys. Rev. B **95**, 054428 (2017).

[19] R. Lavrijsen, D. M. F. Hartmann, A. van den Brink, Y. Yin, B. Barcones, R. A. Duine, M. A. Verheijen, H. J. M. Swagten, and B. Koopmans, Phys. Rev. B **91**, 104414 (2015).

[20] C. Moreau-Luchaire, C. Moutafis, N. Reyren, J. Sampaio, C. A. F. Vaz, N. V. Horne, K. Bouzehouane, K. Garcia, C. Deranlot, P. Warnicke, P. Wohlhüter, J.-M. George, M. Weigand, J. Raabe, V. Cros, and A. Fert, Nat. Nanotechnol. **11**, 444 (2016).

[21] D.-S. Han, N.-H. Kim, J.-S. Kim, Y. Yin, J.-W. Koo, J. Cho, S. Lee, M. Kläui, H. J. M. Swagten, B. Koopmans, and C.-Y. You, Nano Lett. **16**, 4438 (2016).

[22] J. Lucassen, F. Kloodt-Twesten, R. Frömter, H. P. Oepen, R. A. Duine, H. J. M. Swagten, B. Koopmans, and R. Lavrijsen, arXiv:1708.00387.

[23] H. Yang, O. Boulle, V. Cros, A. Fert, and M. Chshiev, arXiv:1603.01847.

[24] C. Quirós, S. M. Valvidares, O. Robach, and S. Ferrer, J. Phys.: Condens. Matter **17**, 5551 (2005).

[25] S. M. Valvidares, J. Dorantes-Dávila, H. Isern, S. Ferrer, and G. M. Pastor, Phys. Rev. B **81**, 024415 (2010).

[26] C. Shern, J. Tsay, H. Her, Y. Wu, and R. Chen, Surf. Sci. **429**, L497 (1999).

[27] J.-W. Lee, J.-R. Jeong, S.-C. Shin, J. Kim, and S.-K. Kim, Phys. Rev. B **66**, 172409 (2002).

[28] R. Allenspach, IBM J. Res. Dev. **44**, 553 (2000).

[29] F. Meier, K. von Bergmann, P. Ferriani, J. Wiebe, M. Bode, K. Hashimoto, S. Heinze, and R. Wiesendanger, Phys. Rev. B **74**, 195411 (2006).

[30] H. Stillrich, C. Menk, R. Frömter, and H. P. Oepen, J. Magn. Magn. Mater. **322**, 1353 (2010).

[31] G. Chen, Arantzazu, A. T. N'Diaye, and A. K. Schmid, Appl. Phys. Lett. **106**, 242404 (2015).

[32] S. Meckler, N. Mikuszeit, A. Preßler, E. Y. Vedmedenko, O. Pietzsch, and R. Wiesendanger, Phys. Rev. Lett. **103**, 157201 (2009).

[33] P. J. A. van Schendel, H. J. Hug, B. Stiefel, S. Martin, and H. J. Güntherodt, J. Appl. Phys. **88**, 435 (2000).

[34] J.-P. Tetienne, T. Hingant, L. Martínez, S. Rohart, A. Thiaville, L. H. Diez, K. Garcia, J.-P. Adam, J.-V. Kim, J.-F. Roch, I. Miron, G. Gaudin, L. Vila, B. Ocker, D. Ravelosona, and V. Jacques, Nat. Commun. **6**, 6733 (2015).

[35] Y. Dovzhenko, F. Casola, S. Schlotter, T. X. Zhou, F. Büttner, R. L. Walsworth, G. S. D. Beach, and A. Yacoby, arXiv:1611.00673.

[36] D. L. Abraham and H. Hopster, Phys. Rev. Lett. **58**, 1352 (1987).

[37] K. Koike, Microscopy **62**, 177 (2013).

[38] B. Boehm, A. Bisig, A. Bischof, G. Stefanou, B. J. Hickey, and R. Allenspach, Phys. Rev. B **95**, 180406(R) (2017).

[39] G. Chen, T. Ma, A. T. N'Diaye, H. Kwon, C. Won, Y. Wu, and A. K. Schmid, Nat. Commun. **4**, 2671 (2013).

[40] R. Frömter, F. Kloodt, S. Röbler, A. Frauen, P. Staeck, D. R. Cavicchia, L. Bocklage, V. Röbisch, E. Quandt, and H. P. Oepen, Appl. Phys. Lett. **108**, 142401 (2016).

[41] J. Tsay and C. Shern, Surf. Sci. **396**, 313 (1998).

[42] E. Lundgren, B. Stanka, M. Schmid, and P. Varga, Phys. Rev. B **62**, 2843 (2000).

[43] P. Grütter and U. T. Dürig, Phys. Rev. B **49**, 2021 (1994).

[44] H. P. Oepen and J. Kirschner, J. Phys., Colloq. **49**, 1853 (1988).

[45] H. Hopster and H. P. Oepen, *Magnetic Microscopy of Nanostructures* (Springer, Berlin/Heidelberg, 2005).

[46] H. P. Oepen and R. Frömter, *Scanning Electron Microscopy with Polarisation Analysis. Handbook of Magnetism and Advanced Magnetic Materials* (Wiley, Chichester, UK, 2007).

[47] R. Frömter, S. Hankemeier, H. P. Oepen, and J. Kirschner, Rev. Sci. Instrum. **82**, 033704 (2011).

[48] R. Frömter, H. Stillrich, C. Menk, and H. P. Oepen, Phys. Rev. Lett. **100**, 207202 (2008).

[49] Due to missing morphology structures on the Pt crystal we were not able to focus accordingly and did not reach the 15-nm resolution of our setup. The beam size for this image is $2\sigma \approx 70$ nm.

[50] S. Rohart and A. Thiaville, Phys. Rev. B **88**, 184422 (2013).

[51] A. Hubert and R. Schäfer, *Magnetic Domains* (Springer, Berlin/Heidelberg, 1998).

[52] B. Lilley, Philos. Mag. **41**, 792 (1950).

[53] The exchange stiffness A can be estimated roughly to scale linearly with the average coordination number of the Co atoms. Although bulk Co has a coordination number of 12, a single monolayer has six neighbor Co atoms. Therefore, the bulk value is rescaled for 7 ML with a coordination of 78/7 atoms. The proximity magnetism of Pt at the interface would only increase this value.

[54] H. A. Alperin, O. Steinsvoll, G. Shirane, and R. Nathans, J. Appl. Phys. **37**, 1052 (1966).

[55] S. P. Vernon, S. M. Lindsay, and M. B. Stearns, Phys. Rev. B **29**, 4439 (1984).

[56] R. Moreno, R. F. L. Evans, S. Khmelevskyi, M. C. Muñoz, R. W. Chantrell, and O. Chubykalo-Fesenko, Phys. Rev. B **94**, 104433 (2016).

[57] H. F. Ding, W. Wulfhekel, and J. Kirschner, Europhys. Lett. **57**, 100 (2002).

[58] S. Pathak and M. Sharma, Adv. Mater. Lett. **3**, 526 (2012).

[59] C. Eyrich, A. Zamani, W. Huttema, M. Arora, D. Harrison, F. Rashidi, D. Broun, B. Heinrich, O. Mryasov, M. Ahlberg, O. Karis, P. E. Jönsson, M. From, X. Zhu, and E. Girt, Phys. Rev. B **90**, 235408 (2014).

[60] S. Tarasenko, A. Stankiewicz, V. Tarasenko, and J. Ferré, J. Magn. Magn. Mater. **189**, 19 (1998).

[61] M. B. Stearns, *Landolt-Börnstein New Series III/19a*, edited by H. P. J. Wijn (Springer, Berlin/Heidelberg, 1986).

[62] At a Co coverage of 1.5 ML the exchange constant A is reduced proportional to the coordination number of the Co atoms to $A = 20$ pJ/m. Using $K_{\text{eff}} = \frac{K_s}{t_{\text{Co}}} + K_V - \frac{1}{2}\mu_0 M_s^2$ for the thickness dependence of the magnetic anisotropy one obtains an upper bound for the anisotropy for low Co coverage (in an e-beam grown [65] as well in sputtered films [30], [66]) leading to $K_{\text{eff}} < 4.8$ MJ/m^3 at 1.5 ML. Here, K_s denotes the surface anisotropy, and $K_V = 5 \times 10^5$ J/m^3 is the volume anisotropy of hcp Co [61], which is in agreement with Ref. [65]. Thus, we obtain $d < 4.3$ meV/Co.

[63] F. Freimuth, S. Blügel, and Y. Mokrousov, J. Phys.: Condens. Matter **26**, 104202 (2014).

[64] H. Yang, A. Thiaville, S. Rohart, A. Fert, and M. Chshiev, Phys. Rev. Lett. **118**, 219901(E) (2017).

[65] N. W. E. McGee, M. T. Johnson, J. J. de Vries, and J. aan de Stegge, J. Appl. Phys. **73**, 3418 (1993).

[66] G. Winkler, A. Kobs, A. Chuvilin, D. Lott, A. Schreyer, and H. P. Oepen, J. Appl. Phys. **117**, 105306 (2015).